URTeC: 3848875

A Success Story: Screening and Optimizing Refracs in the Eagle Ford

Garrett Fowler*[1]; Jose Zaghloul[2]; David Jones[2]; Lindsey Hall-Wiist[2]; Drew Hopson[2]; Sarah Allen[2]; Matteo Picone[3]; Adrian Morales[4]; Matteo Marongiu Porcu[5]; Mark McClure[1]; Dave Ratcliff[1] 1. ResFrac Corporation, 2. Chesapeake Energy, 3. Independent, 4. Independent, 5. Independent

Abstract

In 2019-2020, a modeling study was undertaken to characterize past refrac performance and to provide screening criteria and design improvements for future refracs. In the subsequent years, refrac design changes, informed by modeling, were successfully tested and evaluated in the field.

Two historical wells were selected for the basis of the two-phase study. Well A and Well F were originally completed with 100- and 67-foot cluster spacing, respectively. Each well was refractured after three years of primary production. In Phase One, a model of each well was constructed. Each model was calibrated to the primary production period of the respective well and refrac prediction blind tested against actual refrac performance. In Phase Two, the calibrated models were used to evaluate screening criteria and design changes. Refrac opportunities were screened based on primary cluster spacing and stimulation intensity (proppant/fluid loading). Design changes evaluated included: timing of refrac (delay after start of primary production), cluster spacing, and stimulation intensity.

Modeling of refrac performance demonstrates high production performance predictivity for both wells tested, in line with the significant EUR gains observed in the field.

Model screening and optimization of refracs demonstrated:

- The uplift from refracs is largest with sparsest primary completion cluster spacing, and smallest with tightest primary cluster spacing.
- Increased production with higher refrac proppant/fluid volumes with diminishing returns
- When frac and refrac designs held constant, 30-year EUR was similar whether wells were refrac'ed 1, 3, or 5 years after initial completion.
- For equivalent proppant/fluid volumes, reduced cluster spacing increases short-term productivity but reduces long-term productivity.

Screening criteria and optimization informed future refrac implementation.

This study demonstrates a workflow for characterizing past refrac performance and optimizing future refrac selection and design.

Introduction

In March 2019, Chesapeake Energy acquired substantial acreage rights (~420,000 net acres) in Austin Chalk and Eaglebine reservoirs, located in central Texas. The acreage acquired is in a geographic area called the Brazos River Valley (BRV). Most of the acreage acquired is in Lee, Burleson, Brazos, Madison, Grimes, Robertson, and Washington counties, located some 85 miles East of Austin, Texas. This study focuses on the development of refracture opportunities on existing wells drilled by previous operators in the Eaglebine reservoir.

The Eaglebine is an extensive hydrocarbon play that covers most of our BRV acreage. The Eaglebine section contains the reservoirs between the base of the Austin Chalk and the top of the Buda limestones, the Eagle Ford Shale and Woodbine sandstone, hence its composite name. These reservoirs are sedimentary rock formations of Cenomanian and Turonian ages of the Cretaceous.

Clastic facies dominate the Eagle Ford reservoir in the Brazos River Valley (BRV) area, where the Argillaceous mud rock is the primary facies. The Eagle Ford is a silica and clay rich marine shale with thin interbedded limestones and marls. The Eagle Ford is also organic matter rich in the area under evaluation (BRV), the Eagle Ford lithology is more comparable to the Haynesville shale, in that it is far more clay rich than the Eagle Ford shale of South Texas. This is caused by the proximity of deltas providing sediment to the BRV basin. The high clay content in these rocks impacts mechanical stratigraphy, reservoir quality, and operations.

Fluid maturities vary substantially in the Eaglebine acreage acquired. Fluids range from black oil in the northwest of the acreage and transition gradually to volatile oils, gas-condensate, and dry gas towards the southeast. Some of the most prolific hydrocarbon bearing zones in the Eaglebine are deposited between the depths of 6,000 and 12,000 ft, with thicknesses that combined often exceed 300', porosities ranging from 3 – 10%, and water saturations that range from 20 – 40%.

Upon acquisition of the asset in 2019, Chesapeake Energy evaluated the existing well stock and identified several candidates for re-stimulation. Legacy completions designed between 2014 and 2016 had wide cluster spacing and were pumped with lower sand intensity when compared to more modern completions. Legacy completion designs significantly under-stimulated rock volumes resulting in deferred production and reduced ultimate recoveries.

In December 2019, Chesapeake Energy decided to review two successful refracturing designs pumped by a previous operator. The study described in this paper was initiated in 2020 to evaluate the restimulation of the A and F wells. The goal was to optimize re-stimulation designs for implementation on the upcoming refracturing program. Chesapeake Energy performed a blind test to assess the predictive capabilities of the calibrated model. Chesapeake Energy initially only provided the primary production data for wells A and F and the refrac completion design pumped. Model results satisfactorily matched the production uplift observed after refracturing for both wells.

The study conclusions and recommendations continued to guide the refrac program decisions until the asset divestiture.

Methods

Simulation approach

A fully-coupled fracturing, reservoir, and wellbore simulator was used to model the refrac systems (McClure et al., 2022). All phases of the life of the well are captured in a single, continuous simulation: primary fracturing, shut-in and leak-off, primary production, refracturing, shut-in and leak-off, and secondary production. Hydraulic fractures are represented as true fractures, with apertures (element widths) on the order of millimeters for the entirety of the simulation.

Several features and capabilities of the simulator made it particularly applicable to modeling refracturing:

- Stress changes as a function of pore pressure depletion (poroelastic stress changes) are calculated at every timestep.
- During the refracturing treatment, treating fluids may create new fractures or intersect and flow into existing fractures as a function of the distance to an existing fracture and the degree of depletion of that existing fracture (and commensurate poroelastic stress change). When repressurized above the local Shmin, the fractures created during the primary stimulation may become mechanically open and propagate.
- The simulator handles multiphase (oil, water, gas) inside of the fractures and during leak-off, allowing for accurate characterization of fluid movement when secondary fractures intersect primary fractures.
- The simulator allows for wellbore diameter changes throughout the wellbore and activation/deactivation of clusters with time to represent the correct configurations during primary and secondary fracturing.

Simulation setup

Well A and Well F are sufficiently far apart that they are simulated in separate models constructed using the same geology, fluid model, and geomechanical profiles. The initial properties are populated assuming laterally homogenous properties (“layer-cake” model). A selection of properties are displayed in the figure below.

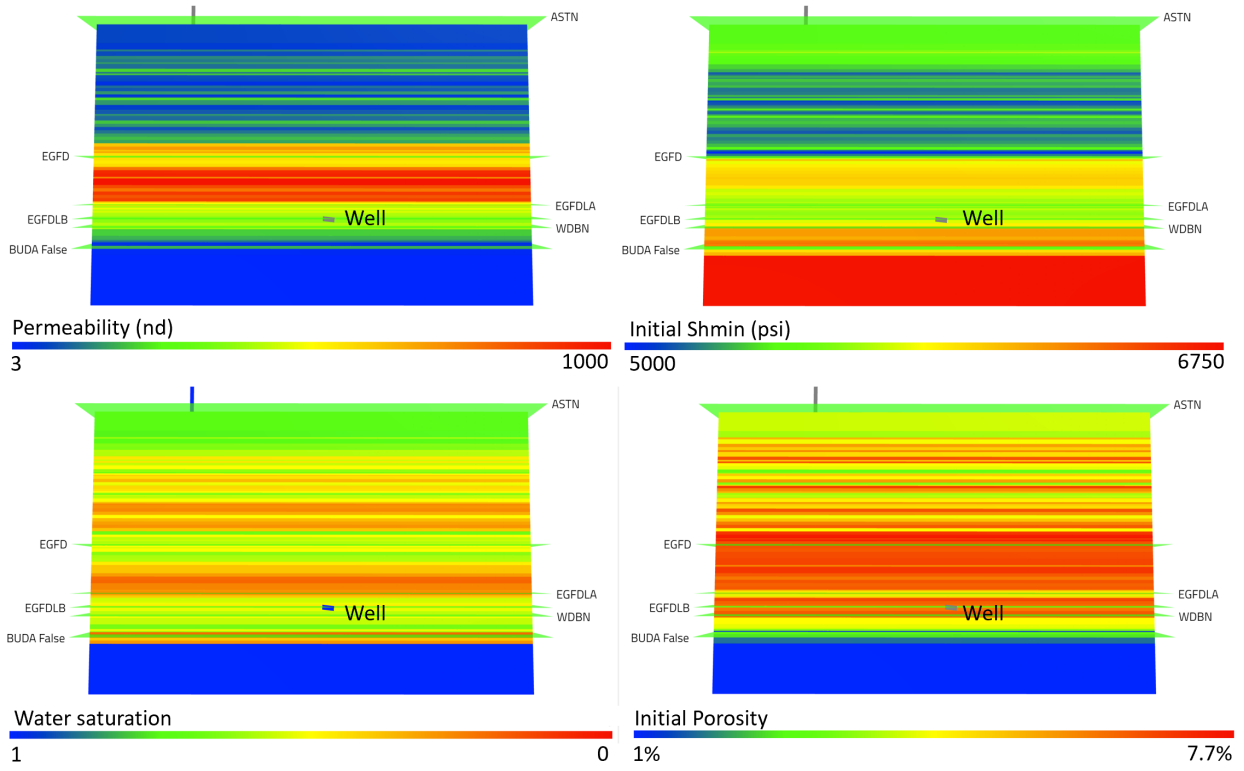

Figure 1.Permeability, water saturation, Shmin (minimal principal stress), and porosity for the chose geomodel.

This area of the Eagle Ford is a black oil. The initial bubble point is ~4000 psi lower than initial reservoir pressure. A black oil fluid model was built based on PVT reports available for the wells in the model.

Well A and Well F were drilled 64 degrees from SHmax. For computational efficiency, the matrix mesh is aligned with SHmax such that fractures will propagate parallel/perpendicular to the matrix mesh. This is not strictly necessary, but improves simulation runtimes.

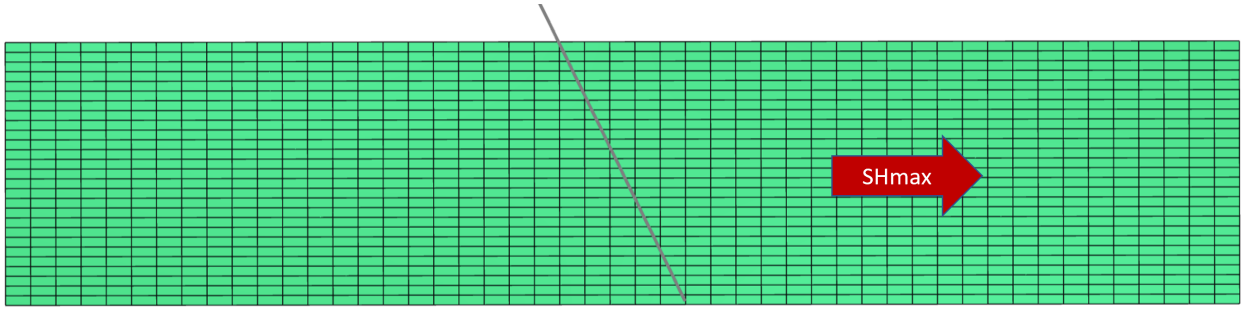

Figure 2. Mesh layout showing orientation of wellbore and matrix meshses. Fractures propagate in the direction of SHmax, parallel/perpendicular to the matrix mesh.

Table 1 below shows the completion parameters for the primary and secondary (refrac) stimulation in both wells. During the shut-in period between primary production and secondary fracturing, the diameter of the lateral sections of Well A and Well F are reduced from 4.778 in (5.5 in casing ID) to 2.99 in (3.5 in casing ID) and the primary perforation clusters deactivated while adding the secondary perforation clusters. Deactivating the primary clusters blocks injection fluid from flowing directly out of primary clusters and into the well; however, fluid can still exit a secondary cluster, flow along the outside of the casing, and into fracture emanating from a primary cluster. This phenomenon is discussed in more detail in the history matching section.

Table 1: Summarized completion parameters for the two wells

		Well A	Well F
Original Stimulation	Primary stage length (ft)	300	280
	Primary clusters spacing (ft)	100	57
	Primary perforations per stage	36	36
	Primary proppant treatment (lbs/ft)	930	950
	Primary fluid system	Hybrid (XL/SLK)	Hybrid (XL/SLK)
	Primary fluid treatment (bbls/ft)	15	18
Refrac Stimulation	Secondary stage length (ft)	180	170
	Secondary cluster spacing (ft)	20	17
	Secondary perforations per stage	64	76
	Secondary proppant treatment (lbs/ft)	2500	3000
	Secondary fluid system	Slickwater	Slickwater
	Secondary fluid treatment (bbls/ft)	54	61

Finally, injection and production control sequences are defined. Both injection periods in both wells are defined using rate controls (inject rate is specified and pressure is matched), while both production periods in both wells are defined using a pressure control (bottom hole pressure, or BHP, is defined and production rates are matched). Primary stimulations in both wells were pumped at a maximum of 50 bpm (barrels per minute), while the refrac stimulation treatments were limited to 58 bpm. The production BHP profile was calculated from production rates and surface pressure measurements. Figure 3 shows a comparison of the calculated BHP and simulation BHP control steps during the primary production period.

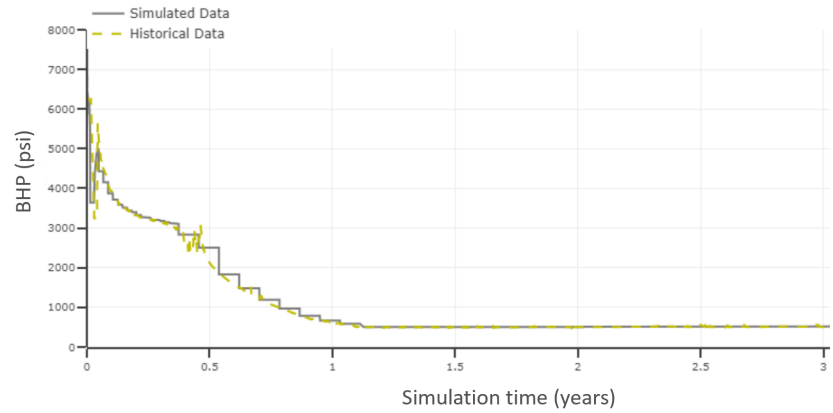

Figure 3. Comparison of calculated BHP (historical data) and simulation BHP control (simulated data)

History Match to Primary Production Period

As all phases of the wells are simulated inside of the coupled-model, fracturing and production characteristics must be matched simultaneously. The interplay of various processes in the subsurface can complicate this process. To streamline and focus the effort, a list of history matching objectives was

created (shown here in Table 2). The idea of creating the table of history match objectives is to distill multifaceted historical observations into a concise list of objectives that characterize the historical behavior.

Table 2: History matching objectives

Historical Observation/Model Objective	Source
Fracture half lengths of 500-1000 ft	Microseismic clouds and observed pressure increases in offset wells
Fractures remain contained in Eagle Ford	No indication of depletion in Chalk above or interference with Chalk wells. Fracture heights limited to 200-300 ft.
Cluster efficiency of 60-70% during primary stimulation	Step rate testing
ISIPs 300-500 psi greater than Shmin	Recorded and interpreted from treating pressures
Strong productivity loss with time	Observed in rate transient analysis of the wells
Production rates and ratios	Daily production testing and allocation

Fowler et al. (2020) outlines a general framework for history matching coupled fracture and reservoir models. That same procedure was used in calibrating the models of Well A and Well F in this study, namely:

1. Match total hydraulic fracture geometries to know calibration points (microseismic, observed frac hits) by adjusting fracture toughness and effective leak-off
2. Calibrate near-well tortuosity, viscous pressure drop inside fractures, and wellbore friction to match treating pressures and instantaneous shut-in pressures (ISIPs)
3. Adjust bulk permeability and effective productive lengths (proppant transport) to match initial deliverability of the well (initial production)
4. Adjust relative permeability and pressure-dependent permeability to match long-term production and production trends

While the outline above appears linear, in practice, there are iterative cycles (for instance, by adjusting bulk permeability, leak-off may be impacted and have to be re-addressed).

Well A and Well F were modeled in separate models. An additional constraint imposed on the modeling process was that the geological parameters between the two models were kept consistent, such that production differences between Well A and Well F models are the consequence of the completion design and drawdown schedule, not arbitrary differences in geologic or petrophysical parameters.

Prediction Validation

An objective of the project was to assess the ability of the models calibrated to the primary production period to predict refrac performance. The production data post-refrac was withheld from the modelers and only the refrac design and post-refrac BHP data were provided. The production predictions from the models of Well A and Well F were then compared to the historical performance of the wells.

Results

History Match Results

A good match to all key history match objectives in Table 2 was achieved using a consistent set of parameters in both Well A and Well F models. The primary history matching parameters and impacts of those parameters were:

- Fracture toughness scaling factor. To match the fracture lengths interpreted from microseismic and frac hits to offset wells, toughness was increased as a function of fracture size (Delaney et al., 1986; Scholz, 2010; McClure et al., 2020). Without toughness scaling, fractures would have been too long.
- Vertical to horizontal fracture toughness ratio. Vertical toughness was elevated above horizontal toughness to match fracture heights. This is hypothesized to account for laminations and bedding planes.

  Figure 4 shows the fracture area after the first three stages in each of the models. The majority of fracture area is contained within the Eagle Ford pay zone. Well F exhibits greater fracture height. The tighter cluster spacing used in the Well F completion (57 ft versus 100 ft) induces more stress shadow between clusters and results in more height growth (these phenomena is discussed by Roussel, 2017).

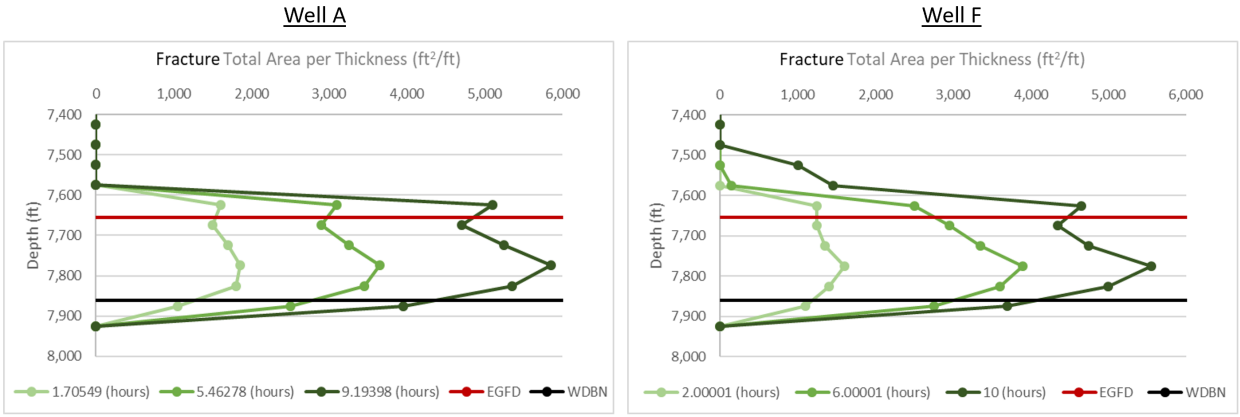

Figure 4. Created fracture area for Well A and Well F after first, second, and third stage fractured in the models

- Accelerated leak-off. A reversible pressure-dependent-permeability (PDP) was necessary to match leak-off and initial water production observations. PDP was set such that permeability was unmodified at and below minimum principal stress (Shmin). Above Shmin, permeability increased as a function of pressure. This is a common practice in models and accounts for leak-off into natural fractures and possible multi-strand fracture propagation (McClure et al., 2020).
- Permeability. The models employed layer-cake, multilayer property distributions. A global permeability multiplier was used to modify permeability of every matrix element in the model uniformly by the same factor and calibrate to total fluid production.
- Relative permeability. Brooks Corey relative permeability end points and exponents were used to tune water cuts and productivity loss with time (loss of oil productivity when BHP went below bubble point).

  Both Well A and Well F exhibited Rate Transient Analysis (RTA) trends that bend upwards. This is a common observation in shale reservoirs (Fowler et al., 2020). Figure 5 shows the correspondence of GOR (gas-oil ratio) increase and bend of the RTA trend (yellow vertical lines demarcate the corresponding time and square-root material balance times). Between 0.25 and 0.5

years into production, the GOR of Well A starts to rise, and there is a corresponding apparent deviation from linear flow in the RTA trend (upward bend) indicating a decrease in oil productivity index. A larger oil relative permeability exponent will cause a relatively larger oil productivity loss for an equivalent change in saturation. In this manner, the upward curvature of the RTA was matched.

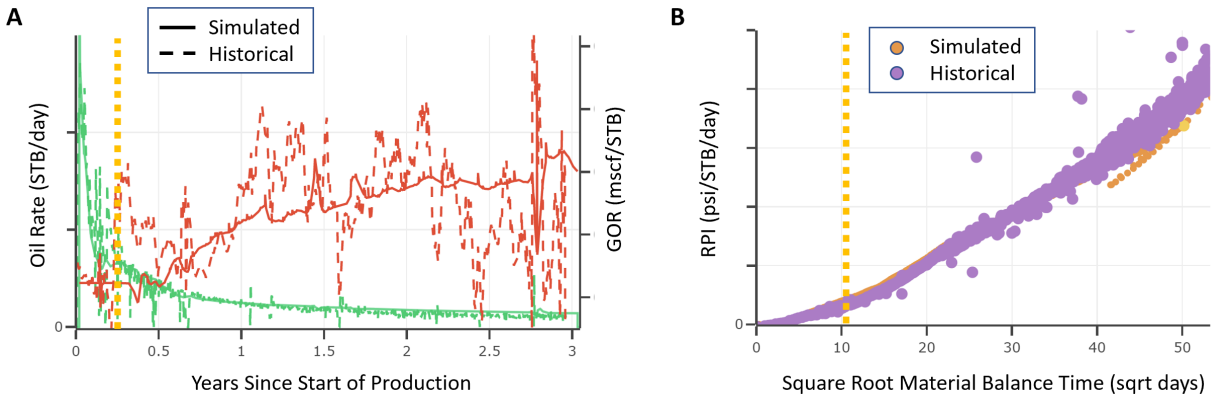

Figure 5. A) Production and B) RTA plots for Well A.The yellow vertical line demarcates the same time in both plots.

Figure 6 shows the final history match to the primary production periods of Well A and Well F. The two models used identical geologic and fracture propagation parameters such that the only differences in the models are the completion designs of Well A and Well F. There are small deviations from the historical data for both wells. These deviations could have easily been minimized by allowing for variation of geologic parameters between the two; however, there was no geologic data to control or indicate differences between the well pads, so to change parameters independently would risk overfitting one or both of the models.

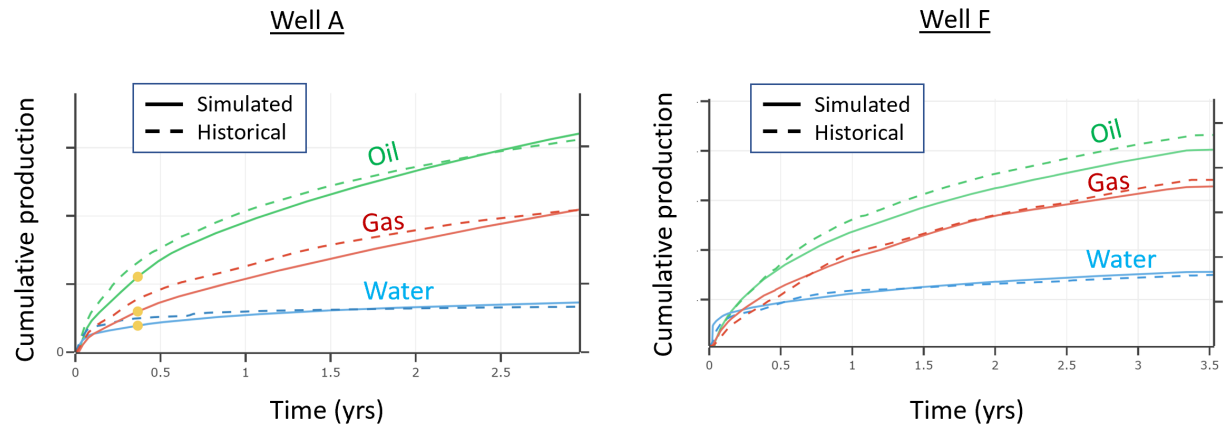

Figure 6. Final history match to the primary production period for Well A (three years) and Well F (3.5 years)

The history match to the primary production periods for Well A and Well F are deemed high quality given the restriction of common parameter sets between the two models.

Predictivity Test

The refrac stimulation design and post-refrac bottomhole pressure during production were provided to the model and oil production compared to actuals. Figure 7 shows the actual and modeled oil rates and cumulative oil production.

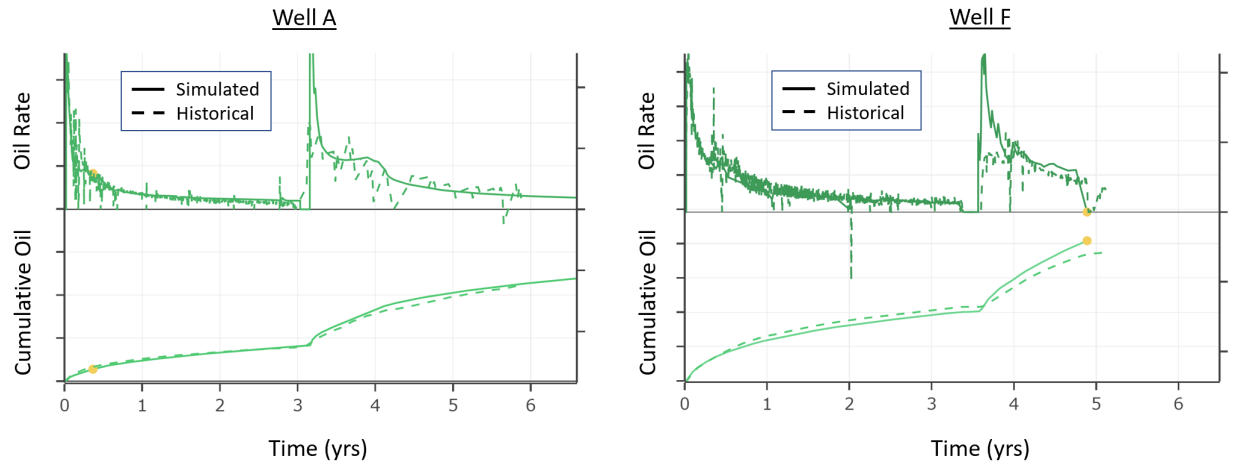

Figure 7. Oil rate and cumulative oil production plots for Well A and Well F for calibration period (before refrac) and blind-test period (after refrac).

Well A exhibits a very close match during both calibration and blind test periods (before and after 3.1 years, respectively). There is a shut-in just after 4 years that is not honored in the simulation; however, the duration of the shut-in is short enough that it is able to be ignored when assessing the overall production trends.

Well F similarly exhibits a close match during the calibration period (before 3.5 years); however, the simulation overpredicts the performance of the refrac. Figure 8 shows that the simulated post-refrac oil production rate is much higher than the actuals for the first six months Well F is online after the refrac. After year 4, the oil rate match for Well F is very good.

BHP calculations were uncertain. It is possible that the calculated BHP used for Well F post-refrac was lower than reality resulting in the higher modeled production. Taking uncertainties into account, the model calibration was considered successful in predicting both Well A and Well F refrac performances and sufficient for predictive modeling and design sensitivities.

The modeling demonstrates that the refrac stimulations improve Well A and Well F performance by adding additional fracture area to each well. The additional fracture area improves production rate immediately after the refrac, but also improves ultimate recovery by stimulating a larger reservoir region: both between the existing primary fractures and further away from the wellbore. Figure 8 shows the depletion around Well F just prior to the refrac and at the end of the simulation. The additional fracture area is clearly observed in the figure. Additionally, a correspondence between the location of the primary fractures and clustering of the secondary fractures is observed. The secondary fractures initiate and

propagate more easily in proximity to the primary depletion due to the reduction in minimum principal stress in this region ("fracture clustering", see also Figure 16).

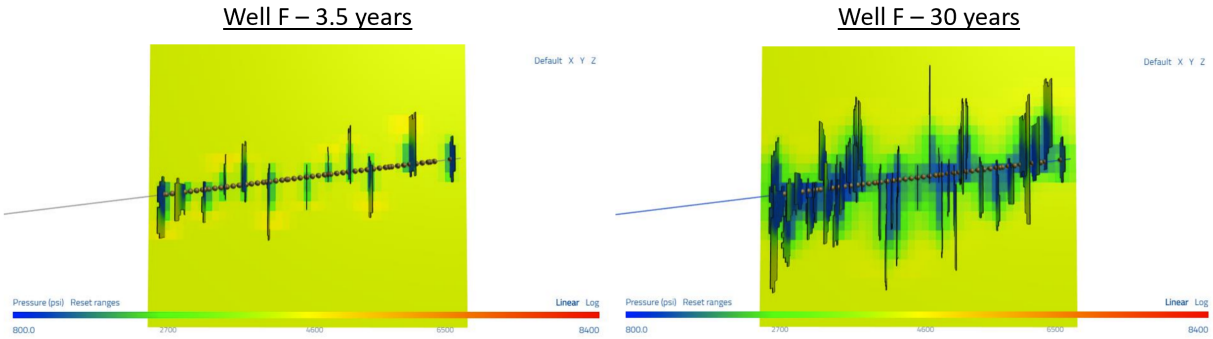

Figure 8. Pressure depletion at 3.5 and 30 years in Well F. 3.5 years is immediately before the refrac stimulation and 30 years

The fracture clustering phenomenon ultimately limits the reservoir contact and success of the refrac, though can be, at least partially, overcome with increased perforation friction.

Refracturing Design Sensitivity

The calibrated model parameters, which were shown to be predictive in the blind-test of refrac performance, were employed to investigate three refrac design choices: primary versus secondary (refrac) cluster spacing, proppant and fluid volumes, and age of primary well prior to refrac. The Well F design was used as the "base case" in all sensitivities as it more closely approximated the available well stock at the time.

Proppant and fluid volumes

Increasing proppant and fluid volumes create additional propped and total fracture area. A sensitivity on job size was performed keeping the primary frac unmodified (see Table 1 above for Well F frac design). The refrac stimulation design was modified between 50% and 200% of the original design, maintaining the same proppant concentration for all cases (i.e., proppant and fluid volumes were changed proportionally). Figure 9 shows how reducing the stimulation volume shrinks the size of the created fractures and ability of those fractures to produce. The green fracture regions in Figure 9 are those most efficiently depleted and are closely correlated to whether those regions are propped. As the stimulation volume and associated

fracture area increase, the portion of the fractures that are unproductive (red to orange) grows. This helps provide intuition for why there are diminishing returns to increasing stimulation job size.

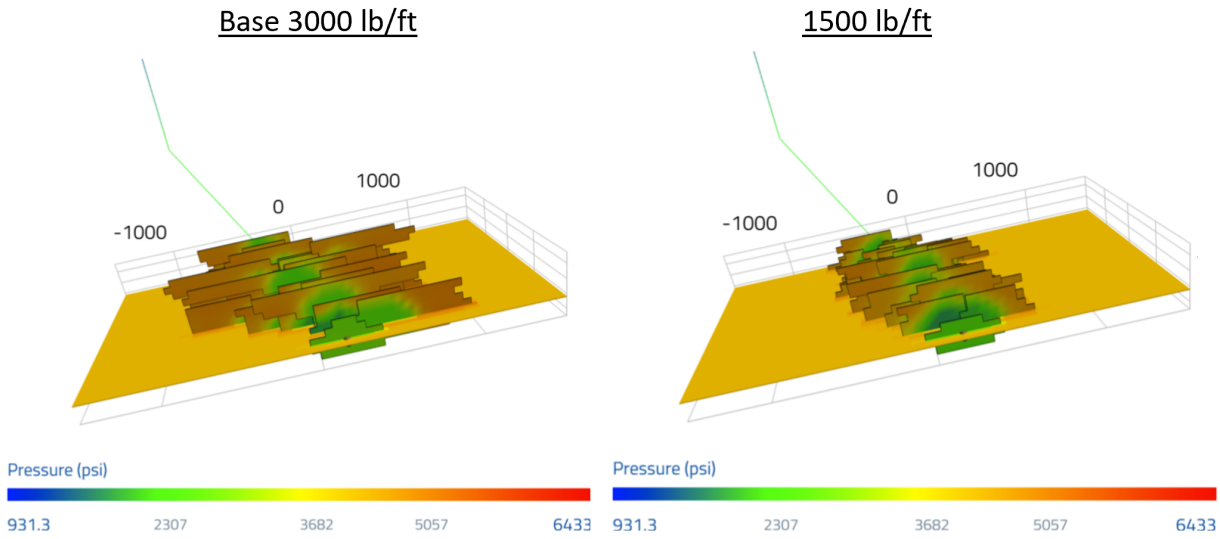

Figure 9. Fracture geometry and pressure in fracutres during post-refrac production

Figure 10 shows diminishing returns for increasing proppant and fluid volumes. As stimulation volumes are increased, there is incrementally less benefit to either propped fracture area creation or cumulative production.

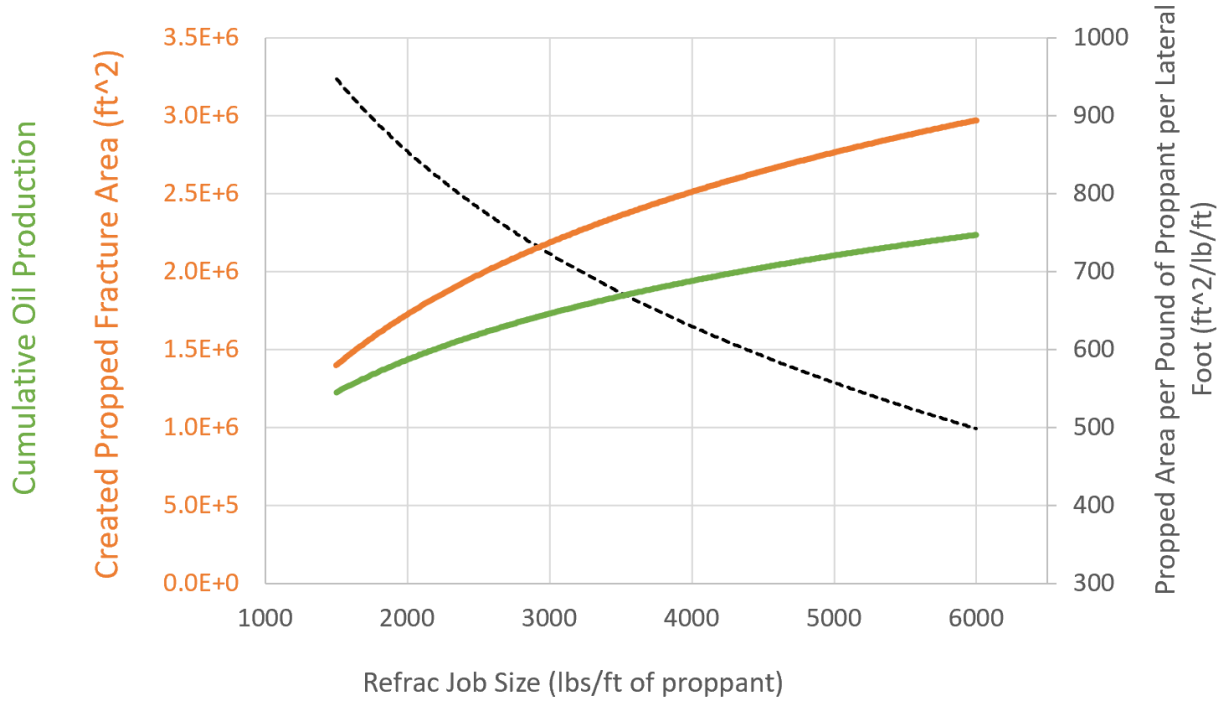

Figure 10. Cumulative production (green) and total created propped area (orange) versus refrac job size. Note: axis values for cumulative oil production have been hidden. The black trend shows the created propped area divided by pounds of proppant per lateral foot.

The black line in Figure 10 shows the total propped area created per pound of proppant pumped per foot of lateral. As the volume of proppant is increased from 1500 lb/ft to 6000 lb/ft, the amount of propped fracture

area created per pound of proppant decreases by nearly 50%. In other words, a 3000 lb/ft refrac completion creates an additional 2.2e6 ft^2 of propped fracture area but doubling the size of the refrac to 6000 lb/ft only results in 40% more propped fracture area (add only 32% higher cumulative production). Figure 11 replots these data using normalized scales. A unit slope (45 degree line) would correspond to a 1:1 relationship between job size and created propped area or cumulative production.

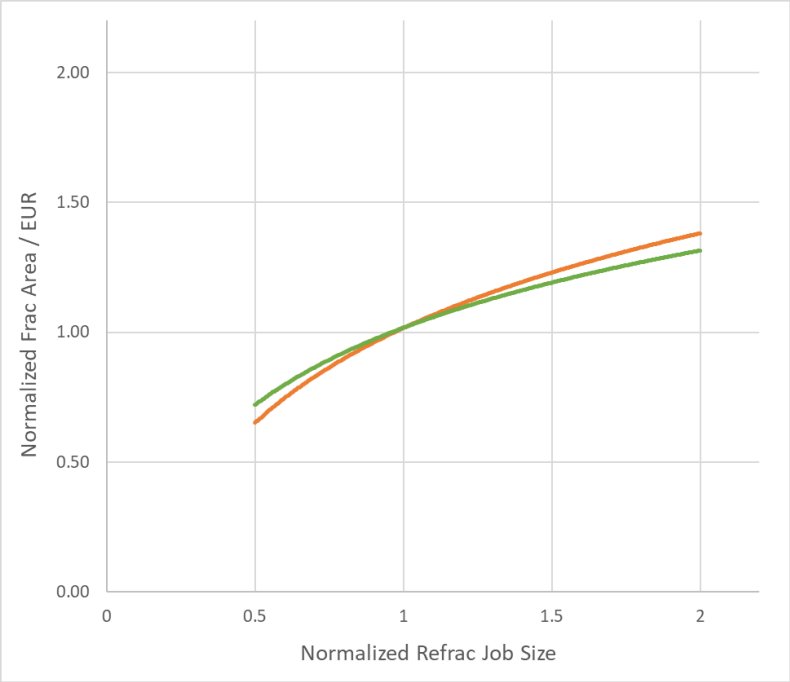

Figure 11. Normalized fracture area and EUR versus normalized job size

Both propped fracture area and cumulative production exhibit normalized trends with less than a unit slope, indicating diminishing returns to larger stimulation volumes. The cumulative production (EUR) trend falls off more rapidly than the propped fracture area trend because not all propped area is equal. The last propped area added is the most likely to be out-of-zone and produce less oil than the first propped area created. Consequently, the normalized cumulative oil trend has a lower slope than the normalized propped area because less propped area is being created per unit of stimulation volume *and* each unit of propped area is less valuable than the prior.

Primary cluster spacing/secondary cluster spacing

There is a natural lower bound on primary cluster spacing beyond which refracs are unlikely to be attractive. The tighter the primary cluster spacing, the less "stranded" resource remains between productive fractures and the associated refrac opportunity is lower.

Figure 12 shows the cumulative oil production for different combinations of primary and refrac cluster spacing, while total proppant and fluid volumes per lateral foot were kept constant for all scenarios. Initial cluster spacings of 50 ft, 25 ft, and 12.5 ft were tested with either 25 ft or 10 ft refrac cluster spacing.

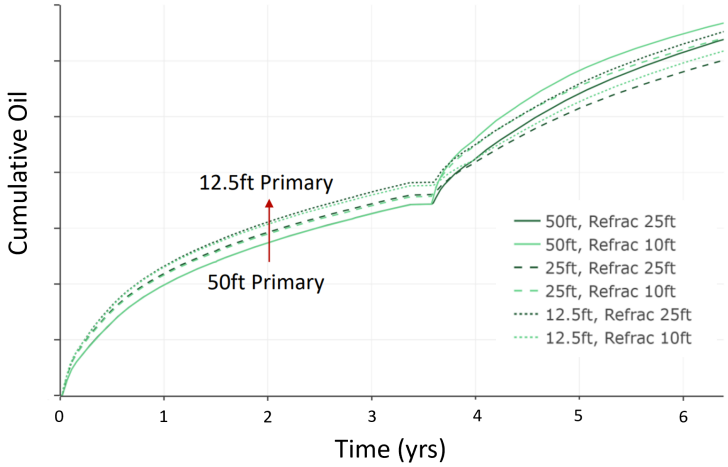

Figure 12. Cumulative oil production for the cases with different primary and secondary cluster spacing

Primary production increases monotonically with decreasing cluster spacing. Fracture area created near the well is more valuable than an equivalent unit of fracture area created far from the well. Decreasing cluster spacing within the range tested redistributes fracture area to the near-well region. Note that the cumulative difference between recovery trends during the primary production period continues to grow up until the point at which the wells are refrac'ed, suggesting that even at 3 years, the production rate of the 12.5 ft cluster spacing scenario is greater than that of the 50 ft cluster spacing scenario.

Tighter primary cluster spacing results in a higher primary recovery factor and less remaining oil to "target" with the refrac. Additionally, depleted primary fractures act as pressure sinks and divert refrac stimulation fluid and proppant. When the primary fracture spacing is tighter, nearly all secondary clusters are within zones of depletion and limited new fracture area is created. Conversely, with sparse primary fracture spacing, some refrac fluid and proppant diverts into depleted fractures, but undepleted regions between the primary fractures allow for new fracture creation. Figure 13 compares the total fracture area of the cases with primary cluster spacing of 12.5 ft and 50 ft when refrac'ed with a 10 ft cluster spacing.

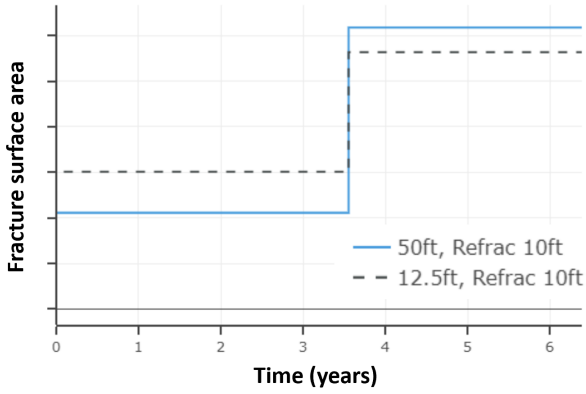

Figure 13. Total created fracture area for scenarios with 12.5 ft and 50 ft initial cluster spacing and refrac'ed with 10 ft cluster spacing

The 12.5 ft primary cluster spacing generates more fracture surface area for the same total volume per lateral foot injected. On average, these fractures are shorter and remain closer to the wellbore than the case with a primary cluster spacing of 50 ft. However, after refrac'ing the well with a 10 ft cluster spacing, the final total fracture surface area is greater in the case with 50 ft initial cluster spacing. In scenario with 50 ft primary cluster spacing, refrac fractures are able to initiate and propagate in virgin rock, allowing for better distribution across the wellbore. Figure 14 shows the final fracture distribution and associated depletion at 30 years.

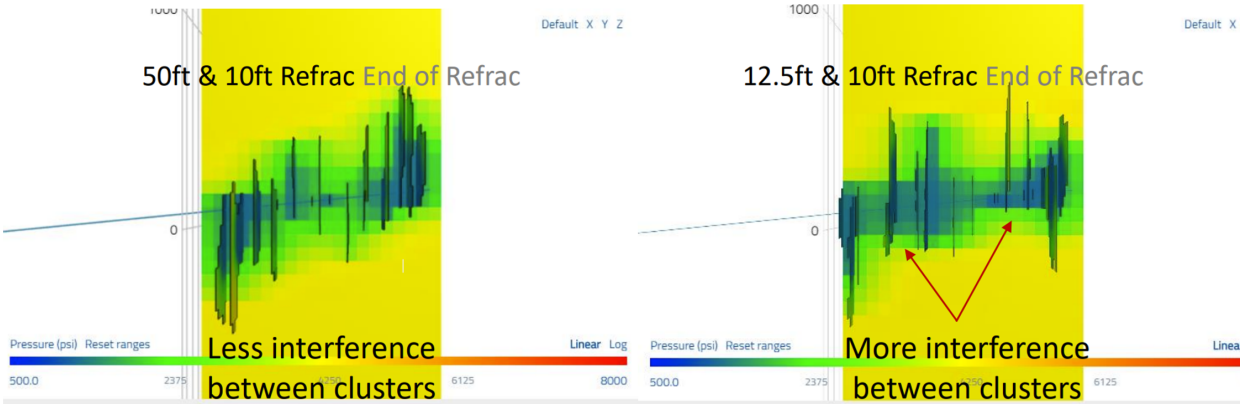

Figure 14. Pressure distribution in the matrix after 30 years of production for cases with either 50 ft or 12.5 ft primary cluster spacing and 10 ft refrac cluster spacing.

Age of primary well

To assess the impact of depletion prior to the refrac, the timing of the refrac in the base model was adjusted to between one and fives years after the start of primary production. The base Well F refrac design is used in all sensitivity scenarios. Figure 15 shows the cumulative production of each scenario over a 20-year period.

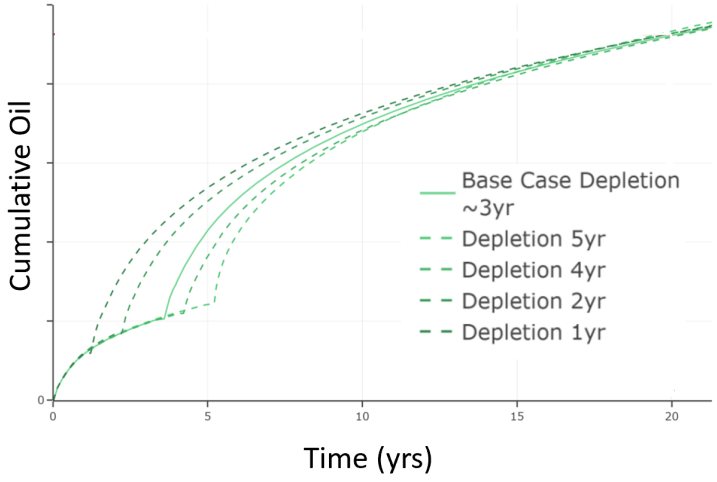

Figure 15. Pressure distribution in the matrix after 30 years of production for cases with either 50 ft or 12.5 ft primary cluster spacing and 10 ft refrac cluster spacing.

All scenarios converge to the same ultimate recovery 20 years after the start of primary production (15 to 19 years after the refrac stimulation. This indicates that for under stimulated wells, the ultimate recovery of the well is insensitive to the exact timing of the refrac. The timing of the refrac can then be optimized from an economic (time-value of revenues, variable cost inputs) and operational standpoint. It is noted

that as depletion is increased beyond the range tested, the effect of fracture clustering (discussed below) would be expected to be greater and ultimately detrimental to ultimate recovery when primary depletion sufficiently large. Inspection of Figure 15 shows that the refrac adds significant reserves to the well within the range tested, with EUR of the refrac approximately three times higher than the projected EUR from the primary production period.

Discussion

This study addressed several facets of the very broad topic of refracturing legacy wells. In the bullets below, we discuss nuance not explicitly addressed in the material above.

- Outside-of-casing communication. Communication pathways outside of the casing, where fluid and proppant could exit one perforation and travel into the nearfield region of an adjacent cluster, may exist. The presence and intensity of these communication pathways may be inferred from pump-down diagnostics (Cramer et al., 2020). Communication behind casing was not measured in the subject wells and so a default value was used, previously calibrated in other studies, allowing for transmissibility outside of the casing between clusters with-in 30 feet of each other.
- Fracture clustering. Figure 16 below superimposes the primary and secondary fracture geometries of Well F. The primary depletion causes a poro-elastic stress reduction in the vicinity primary fractures. The normal stress on the primary fracture is less allowing for easier fracture reactivation. Additionally, the secondary fractures cluster around the primary fractures as clusters within this depleted region initiate and propagate more easily due to the lower stress. This may be overcome to some degree with limited entry perforating.

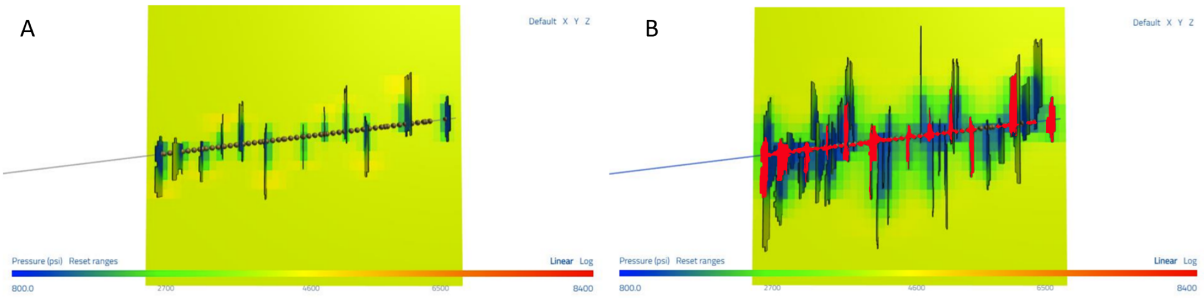

Figure 16. A) fracture geometry and pressure depletion of Well F prior to refrac. B) primary fractures and depletion in red overlaid on fracture geometry and pressure depletion 20 years after the refrac in Well F

- Targeted perforating. The simulations demonstrate localization of refrac proppant and fluid into regions depleted during primary production (so called fracture clustering, above). If depleted regions could be cost-effectively identified prior to the refrac completion, refrac performance could likely be improved yet further.
- Planarity of fractures. Both models in this study assumed that fractures propagate in the direction of initial maximum horizontal principal stress. Depletion can induce a rotation in the principal stress directions and simulation model can calculate this reorientation. However, the degree of stress reorientation is a function of anisotropy between minimum and maximum horizontal stresses and it is inherently difficult to accurately estimate of maximum horizontal stress. There was no evidence of fracture turning in the field data, so it was assumed that stress anisotropy was sufficiently high that no rotation occurred.
- Offset wells. Well A and Well F are unbounded wells, with offset wells sufficiently far away that they could be neglected in this analysis. Production and financial returns of the refrac would be limited if offsetting wells of the same or a subsequent generation existed adjacent to the refrac

well as opposed to the case where the refrac well is unbounded. This screening criterion was not investigated in this study, but prior to refrac'ing a well in close proximity to other wells, the effect of the bounding wells should be investigated.

- Fracture damage. Some basins have exhibited parent-well productivity declines above and beyond that expected from interference when offsetting child wells are frac'ed (McClure et al., 2023; Ratcliff et al., 2022; Rassenfoss, 2020; Nieto et al., 2018; King et al., 2017; Miller et al., 2016). These effects were not observed in this Eagle Ford data set. However, if investigating refracs in basins where fracture damage mechanisms are more prevalent (Woodford, Meramec, Montney, and others) then these damage mechanisms may negatively impact the results of refracs similar to performance limitations observed on children wells. Fowler et al. (2022) discusses how these effects can be incorporated into a simulation.
- Diverter. The use of bullhead diverter was briefly investigated, though was quickly ruled out. Even under optimistic assumptions of ideal diverter distribution and blockage, production uplift was limited. The diverter scenarios rely on extending existing fractures and restoring/adding conductivity to those fractures, and therefore are not adding significant new reservoir area. Some historical cases in the literature have shown more substantial uplift from bullhead diverter refracs so it is suggested that further investigation into alternative mechanisms (wellbore cleanout, suppression of gas in the matrix, etc.) be conducted.

Model Modernization

The study was originally concluded in 2020. In preparation for this paper, the Well A model was updated to conform with the latest numerical updates in the three years since the model was originally built and calibrated. The most substantial of these updates is the use of a continuous fracture front tracking algorithm (Donstov, 2022). Figure 17 below shows the comparison of the original and continuous fracture models.

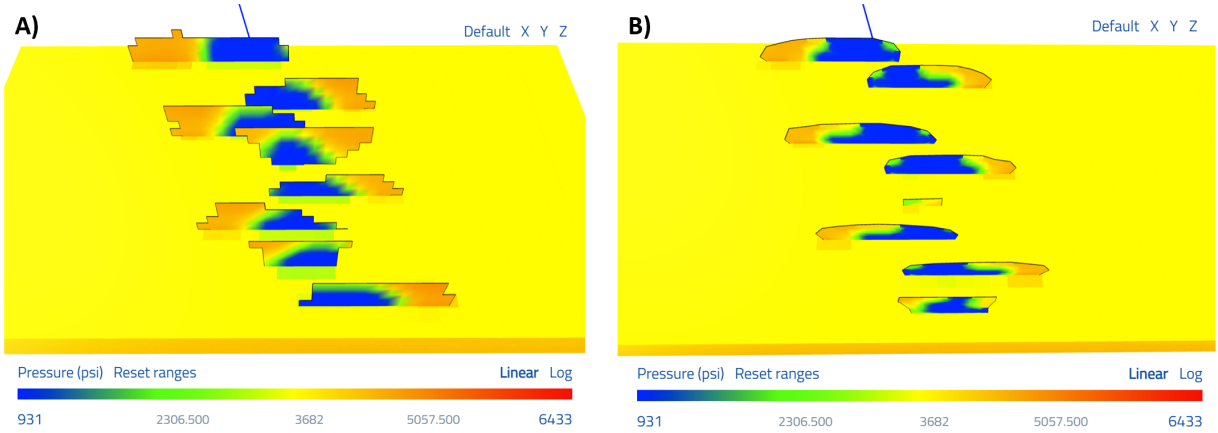

Figure 17. A) original Well A model from 2019/2020 with discrete fracture elements B) updated model from 2023 with continuous fracture front elements

In the updated, continuous fracture front model partial fracture elements are allowed to form, smoothing the edges of the fractures and allowing for coarser fracture meshes while maintaining resolution. The continuous fracture front algorithm and additional numerical updates reduced the runtime of the Well A model by 70%.

Updates to model did slightly alter model results, requiring modest recalibration to the historical data. The model was recalibrated to the historical data through 2020 by adjusting relative fracture toughness to match the same fracture size distributions of the original model and permeability and relative permeability

adjustments to fine tune production back to the original model. The updated model was then used to predict production data from 2020 to 2023 and compared to the actual data, as it is shown in Figure 18. Results compared favorably to the historical data, further establishing confidence in the use of the model and optimization results.

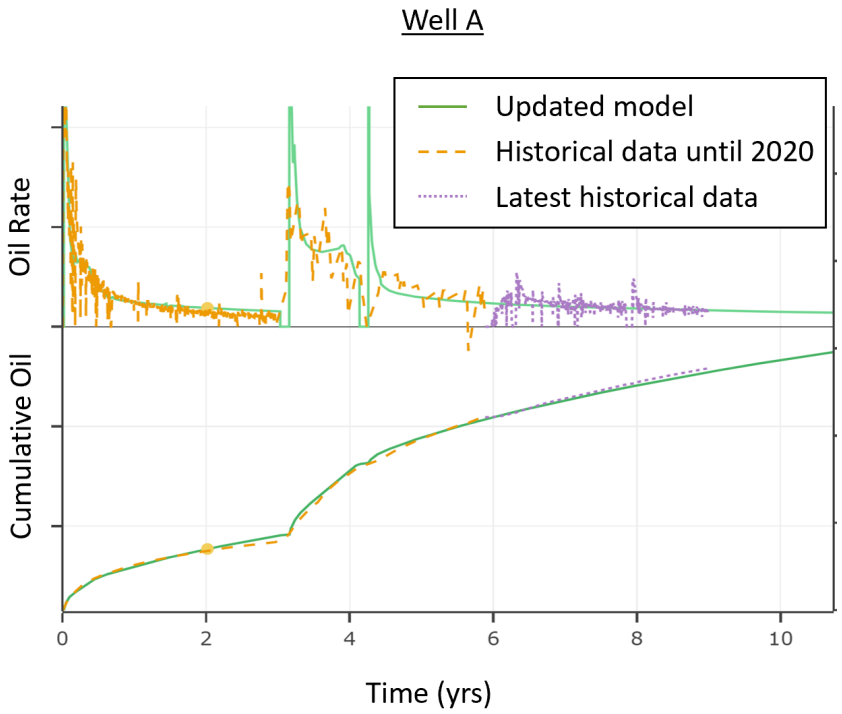

Figure 18. Production predictions from updated model. The updated model was adjusted to match the original model from 2020 and then tested against the data from 2020 to 2023.

Conclusions

This study investigated the success of two refracs in the Eagle Ford and sensitivity of well productivity to specific refrac design decisions. The two historical cases and sensitivities all demonstrated significant resource additions from the refrac, with the two historical cases being financial successes as well.

- The refracs presented in this study were technical and economic successes, approximately tripling the recovery of the subject wells.
- Calibrating to the primary production of multiple wells constrained uncertain model parameters and allowed the models to be predictive of refrac performance when blind-tested.
- Performance differences between Well A and Well F are driven by the stimulation design more than geologic differences. Well performance was properly matched for both single well models (Parents) having consistent geology.
- Incorporating depletion and poro-elastic stress changes allow the models to capture dominant mechanisms at play.
- Refrac opportunity is a function of the primary stimulation design (volumes, cluster spacing, depletion history) as well as mechanical integrity (not investigated in this study), and screening criteria can be cost-effectively established using computational models.

References

Cramer, David, Jon Snyder, and Junjing Zhang. 2020. Pump-down diagnostics for plug-and-perf treatments. Paper SPE-201376-MS presented at the SPE Annual Technical Conference & Exhibition.

Delaney, Paul T., David D. Pollard, Joseph I. Ziony, and Edwin H. McKee. 1986. Field relations between dikes and joints: emplacement processes and paleostress analysis. Journal of Geophysical Research 91(B5): 4920-4938.

Dontsov, Egor. 2022. A continuous fracture front tracking algorithm with multi layer tip elements (MuLTipEl) for a plane strain hydraulic fracture, Journal of Petroleum Science and Engineering, Volume 217, 2022, 110841, ISSN 0920-4105, https://doi.org/10.1016/j.petrol.2022.110841.

Fowler, G., McClure, M. & Allen, J. (2020a). RTA Assisted History Matching with a Combined Hydraulic Fracturing and Reservoir Simulator. Paper SPE-199149-MS presented at the SPE Virtual Latin American and Caribbean Petroleum Engineering Conference.

Fowler, Garrett, Dave Ratcliff, and Mark McClure. 2022. Modeling Frac Hits: Mechanisms For Damage Versus Uplift, SPE-22194-MS. Paper presented at the 2022 International Petroleum Technology Conference.

King, Rainbolt, and Swanson. 2017. Frac hit induced production losses: evaluating root causes, damage location, possible prevention methods and success of remedial treatments. SPE-187192-MS.

McClure, Mark, Charles Kang, Chris Hewson, Soma Medam, Egor Dontsov, and Ankush Singh. 2022. ResFrac Technical Writeup. 12th Edition. arXiv:1804.02092. https://doi.org/10.48550/arXiv.1804.02092.

McClure, Mark, Matteo Picone, Garrett Fowler, Dave Ratcliff, Charles Kang, Soma Medam, and Joe Frantz. 2020. Nuances and frequently asked questions in field-scale hydraulic fracture modeling. Paper SPE 199726-MS presented at the Hydrauic Fracturing Technology Conference, The Woodlands, TX.

McClure, Mark, M.L. Albrecht, SM Energy; C. Bernet, Ovintiv; C.L. Cipolla, Hess Corp.; K. Etcheverry, Ovintiv; G. Fowler, ResFrac Corporation; A. Fuhr, SM Energy; A. Gherabati, Ovintiv; M. Johnston, ARC Resources Ltd; P. Kaufman, Hess Corporation; M. Mackay, Birchcliff Energy Ltd; M.P. McKimmy, Hess Corp.; C. Miranda, Hess Corporation; C. Molina, Ovintiv; C.G. Ponners, D.R. Ratcliff, J. Rondon, A. Singh, ResFrac Corporation; R. Sinha, A. Sung, Marathon Oil; J. Xu, Marathon Oil Co; J. Yeo, Birchcliff Energy Ltd; R.B. Zinselmeyer, ARC Resources Ltd. 2023. “Results From a Collaborative Industry Study on Parent/Child Interactions". Paper presented at the SPE Hydraulic Fracturing Technology Conference and Exhibition, The Woodlands, TX.

Miller, Lindsay, Baihly, and Xu. 2016. Parent well refracturing: economic safety nets in an uneconomic market. SPE-180200-MS.

Nieto, John, Graham Janega, Bogdan Batlai, and Hugo Martinez. 2018. An integrated approach to optimizing completions and protecting parent wells in the Montney Formation, N.E.B.C. URTeC-2902707

Rassenfoss. 2020. Solving the gummy bears mystery may unlock greater shale production. Journal of Petroleum Technology.

Ratcliff, Dave, Mark McClure, Garrett Fowler, Brendan Elliot, Austin Qualls. 2022. Modeling Parent Child Well Interactions. Paper presented at the Hydraulic Fracture Technology Conference, Woodlands, TX.

Roussel, Nicolas P. "Analyzing ISIP Stage-by-Stage Escalation to Determine Fracture Height and Horizontal-Stress Anisotropy." Paper presented at the SPE Hydraulic Fracturing Technology Conference and Exhibition, The Woodlands, Texas, USA, January 2017. doi: https://doi.org/10.2118/184865-MS

Scholz, Christopher H. 2010. A note on the scaling relations for opening mode fractures in rock. Journal of Structural Geology.